



# Moving target imaging of a dual-channel ISAL with binary phase shift keying signals and large squint angles

ANJING CUI,<sup>1,2</sup> DAOJNG LI,<sup>1,\*</sup> JIANG WU,<sup>1,2</sup> KAI ZHOU,<sup>1,2</sup> JINGHAN GAO,<sup>1,2</sup> MING QIAO,<sup>1</sup> SHUMEI WU,<sup>1</sup> YEFEI WANG,<sup>2,3</sup> AND YUAN YAO<sup>3</sup>

<sup>1</sup>Key Laboratory of Science and Technology on Microwave Imaging, Aerospace Information Research Institute, Chinese Academy of Sciences, Beijing, 100190, China

<sup>2</sup>University of Chinese Academy of Sciences, Beijing, 100049, China

<sup>3</sup>Changchun Institute of Optics, Fine Mechanics and Physics, Chinese Academy of Sciences, Changchun, Jilin, 130033, China

\*Corresponding author: lidj@mail.ie.ac.cn

Received 17 March 2022; revised 21 May 2022; accepted 30 May 2022; posted 31 May 2022; published 16 June 2022

A dual-channel inverse synthetic aperture ladar imaging experimental system based on wide-pulse binary phase coded signals and its moving target imaging are introduced. The analysis, simulation, and experimental data processing results of binary phase coded signal Doppler compensation and pulse compression are included. The method of motion phase error estimation based on interferometric processing and the imaging method with small computation in the case of large squint angles are proposed, and the simulation results are presented. The effectiveness of the imaging method is verified by experimental data processing. Doppler frequency curves are estimated based on time-frequency analysis of echo signals, and the coarse compensation of motion phase error is realized. According to the interferometric phase and coherence coefficient of dual-channel echo signals' time-frequency analysis, the coherence of the dual-channel echo signals is checked, and along-track interferometry can be applied to the precise compensation. The stable interferometric phase and increased coherence coefficient of actual dual-channel data imaging results indicate the effectiveness of the motion phase error compensation method proposed. Considering characteristics of inverse synthetic aperture ladar (ISAL) imaging, after dividing echo signals into multiple sub-apertures, range-Doppler algorithm and sub-aperture stitching are adopted, the stitched image is corrected geometrically through Stolt transformation, and the computation is reduced. © 2022 Optica Publishing Group

<https://doi.org/10.1364/AO.458595>

## 1. INTRODUCTION

Compared with microwave synthetic aperture radar (SAR), synthetic aperture ladar (SAL) and inverse synthetic aperture ladar (ISAL) have characteristics of narrow beam and concentrated energy, and can be used in long-range detection of targets with small fields of view, which makes it possible to apply ISAL to geosynchronously (GEO) orbit target detection and imaging based on the ground-based platform. Research on SAL and ISAL has attracted extensive attention. To realize high resolution imaging, SAL and ISAL require wideband transmitting signals.

With clear characteristics and demodulation modes, the linear frequency modulation signal (LFM signal) has been widely applied to microwave SAR. In [1,2], the LFM signal is applied in SAL, but it has influence on imaging because of its poor linearity in the laser band. The phase coded signal has the characteristics of large time-bandwidth product, good autocorrelation, and low sidelobe, can be formed by high-speed broadband laser phase modulators, and is relatively easy to generate. Therefore,

the phase coded signal has application value in SAL/ISAL imaging.

Lockheed Martin completed the SAL imaging experiment with the phase coded signal as the transmitting signal in 2009 [3] and the airborne SAL imaging based on 20 ns pulse width, 7 GHz bandwidth in-pulse phase coded signal in 2011 [4]. In [5], the ISAL imaging experiment based on 1024 code length M-sequence binary phase coded signal is reported in 2018. In [6–8], the imaging performance of SAL with phase modulated signals, including the binary phase shift keying (BPSK) signal, the synthetic frequency stepping LFM signal and the intensity encoding are analyzed, respectively.

In [9–11], the translation target motion phase error estimation methods based on the dual-channel and multi-channel echo signal are introduced. The method of rotation targeting motion phase error on the basis of multi-channel echo signals is proposed in [12]. When the dual-channel echo signals have

good coherence, it is feasible to estimate motion phase error through interferometric processing.

A dual-channel ISAL imaging experimental system with the 2000 code length and 1  $\mu$ s pulse width BPSK signal, a motion phase error compensation method based on interferometric processing and an imaging algorithm with small computation and large squint angles are introduced in this paper. The results of simulation analysis and experimental data processing are provided.

## 2. EXPERIMENTAL SYSTEM AND THE BPSK SIGNAL PROCESSING

### A. Experimental System Structure

The BPSK signal dual-channel ISAL experimental system is mainly composed of the laser, formation, and acquisition module of the signal and the optical system. A short-wave infrared camera is set to observe the target. The system block diagram and physical photos are shown in Figs. 1 and 2.

The optical system consists of two receiving fiber collimators and one transmitting fiber collimator. Both of the transmitting and receiving collimators adopt cylindrical lens, and the beams are expanded in pitching direction. After beam expansion, the azimuth beam width of the transmitting lens is 1.2 mrad, the pitching beam width is greater than 34 mrad, the azimuth beam width of the receiving lens is 1.5 mrad, and the pitching beam width is 35 mrad, with 0.3 mrad being the ideal receiving collimator beam width. The equivalent along-track baseline length of the two receiving telescopes is 8.15 mm.

The central wavelength of the laser is 1.55  $\mu$ m, the peak power of the laser is 10 W, and the laser output is linearly polarized. The pulse width and pulse repetition rate (PRF) of the transmitting signal is 1  $\mu$ s and 100 kHz. The analog-to-digital (AD) sampling rate of two receiving channels and one

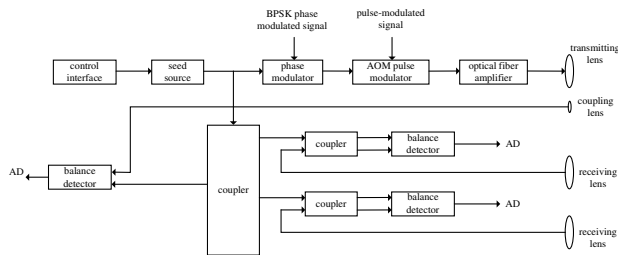


Fig. 1. Block diagram of the experimental system.



Fig. 2. Photo of the experimental system.

transmitting reference channel is 4 GS/s. At the same time, a transmitting reference channel is set up in the test system to enable pulse compression of the phase coded signal.

### B. Pulse Compression of the BPSK Signal

The laser takes the BPSK signal as the transmitting signal and sets the signal pulse width of 1  $\mu$ s, subcode width of 0.5 ns, code length of 2000, and bandwidth of 2 GHz. After Hilbert transform, the equivalent bandwidth of the complex signal is 1 GHz, and the corresponding resolution is 15 cm.

The BPSK signal used in the experiment is modulated according to M-sequence. The period of M-sequence is  $(2^n - 1)$ , where  $n$  is the step of the binary shift register, and the usage of M-sequence can be divided into periodic and aperiodic methods. The first 2000 chips of the M-sequence with a period of 2047 are intercepted and used in the experiment, which satisfies the aperiodic method of M-sequence with long code length [13], and the main-sidelobe ratio of the autocorrelation result is  $\sqrt{N}$ , which means that the sidelobe is  $20\log_{10}(1/\sqrt{N})$ , where  $N$  presents the code length. Therefore, pulse compression of BPSK signals with long code length can suppress the sidelobe effectively. When the code length is 2000, the main-sidelobe ratio of the signal is about 33 dB, and its simulation is shown in Fig. 3.

The BPSK signal and pulse-modulated signal generated by the signal generation and acquisition module through digital-analog converter (DAC) are shown in Fig. 4.

The echo signal of the high-reflectivity static target (a tree with high-reflectivity paper), which is about 70 m away from the transmitting and receiving lens, the corresponding transmitting reference signal, and their pulse compression result are shown in Fig. 5. The main-sidelobe ratio of the pulse compression result is about 25 dB.

BPSK signals have the characteristic of Doppler sensitivity [14–16], and the Doppler tolerance is determined by the pulse width. The Doppler tolerance is the Doppler frequency when the main-sidelobe ratio drops 3.96 dB due to the Doppler sensitivity. For phase coded signals, the formula of Doppler tolerance is as follows:

$$f_{-3.96 \text{ dB}} = \frac{1}{2T} = \frac{1}{2N\tau}, \quad (1)$$

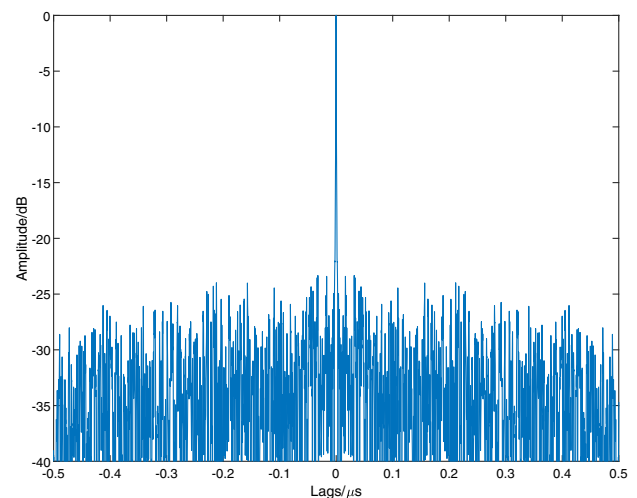


Fig. 3. Pulse compression simulation of the BPSK signal.

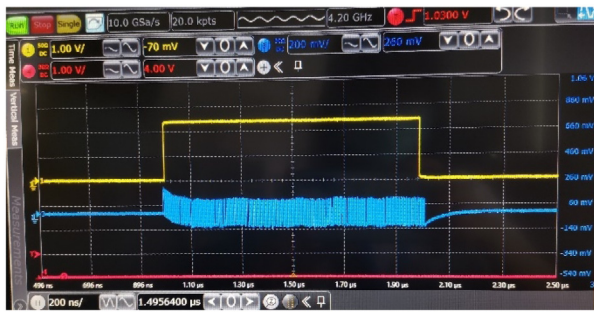


Fig. 4. BPSK signal and pulse-modulated signal.

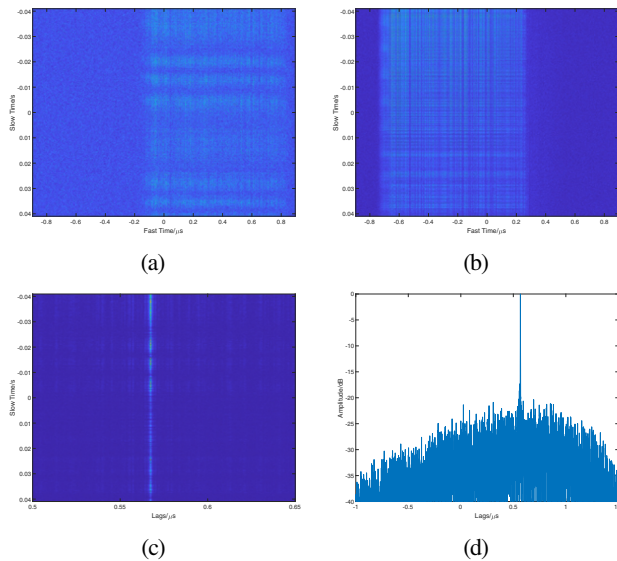


Fig. 5. Echo signal, corresponding transmitting reference signal, and the pulse compression result of the static target. (a) Echo signal. (b) Transmitting reference signal. (c) Pulse compression result of the echo signal in range direction. (d) Pulse compression result section of the echo signal in range direction.

where  $T$  is pulse width of the signal,  $N$  is the code length, and  $\tau$  is the subcode width. According to Eq. (1), the Doppler tolerance of the BPSK signal with pulse width of  $1 \mu\text{s}$  is 500 kHz. For the echo signal of the moving target, when the radial velocity of the target reaches 0.3875 m/s, the transmitting reference signal or the echo signal need Doppler compensation before pulse compression.

The following two methods are combined to achieve the estimation of Doppler frequency according to echo signals:

- Estimate the approximate Doppler frequency based on velocity of the cooperative target;
- Compensate the echo signal with the approximate Doppler frequency, and adjust the Doppler frequency in a small range to ensure that the Doppler frequency center of the processed echo signal is 0, so as to obtain the accurate Doppler frequency.

When the radial velocity of the moving target (a cooperative car with high-reflectivity paper) is 3.24 m/s and the corresponding Doppler frequency is 4.18 MHz, the Doppler

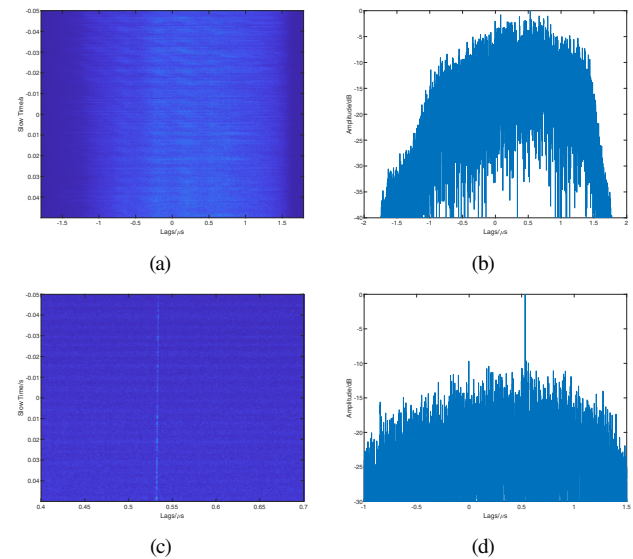


Fig. 6. Pulse compression in range direction of the transmitting reference and the echo signal with/without Doppler compensation. (a) Pulse compression in range direction without Doppler compensation. (b) Section of panel (a). (c) Pulse compression in range direction with Doppler compensation. (d) Section of panel (c).

compensation phase needs to be introduced to the transmitting reference signal. As shown in Fig. 6, the pulse compression has no obvious effect without Doppler compensation, and the main-sidelobe ratio of the pulse compression result with Doppler compensation is 15 dB.

Doppler compensation and pulse compression of BPSK signals enable the range-direction focus of ISAL imaging results and compensate the radial motion phase of moving target echo signals, which lays the foundation for the following motion phase error compensation.

### 3. ISAL IMAGING PROCESS WITH LARGE SQUINT ANGLES

In the case of microwave band SAR imaging with large squint angles and a large-scale scene in azimuth direction, limited PRF is set to ensure the breadth, and upsampling in slow time direction and the omega-K algorithm are generally applied to imaging. In this paper, the synthetic aperture length is assumed to be 0.3 m according to the azimuth beam width, and the azimuth resolution is 1.45 mm. During ISAL moving target imaging, there are some problems such as high Doppler frequency and a small azimuth scene covered within one synthetic aperture time, so the image generated by data of one synthetic aperture has limited application value. In order to avoid the upsampling of the echo signal and reduce the computation, the echo signal with rough Doppler frequency compensation is divided into multiple sub-apertures, and motion phase error compensation and further Doppler frequency compensation are applied to sub-apertures. The range-Doppler (RD) algorithm is used to realize the sub-aperture imaging, respectively. When length of the echo signal is much larger than the synthetic aperture length, the stitched complex image has a geometric

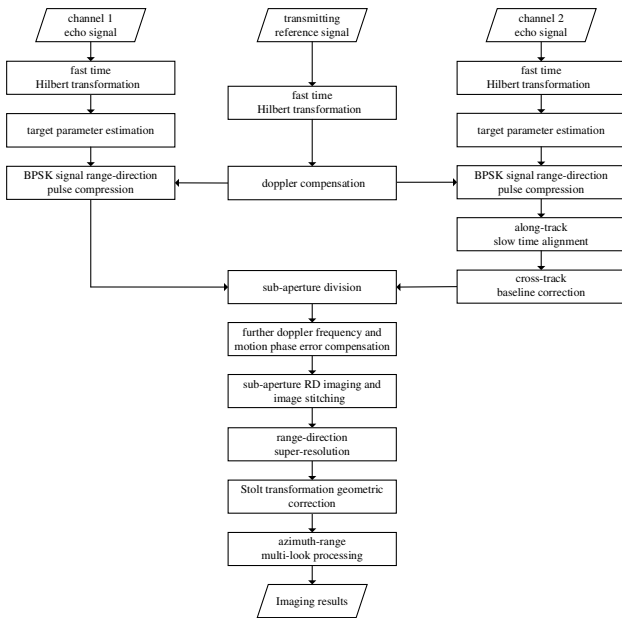


Fig. 7. Spatial domain imaging of laser echo signals.

distortion problem, and the geometric correction can be realized through Stolt transformation.

In the case of large squint angles, the spatial domain imaging of laser echo signals is shown in Fig. 7.

### A. Pretreatment of Laser Echo Signals

The dual-channel echo signals and the transmitting reference signal obtained by the experimental system are transformed to complex signals through fast time Hilbert transform. According to the performance of BPSK signals in Section 2.B, we apply range-direction pulse compression to the transmitting reference signal with Doppler compensation and dual-channel echo signals. We estimate the radial velocity of the target through the Doppler center frequency and the performance of the pulse compression of echo signals. We estimate the transverse velocity of the target through the time-frequency analysis of echo signals. Alignment of dual-channel echo signals in slow time direction is completed based on the equivalent along-track baseline length and the speed of the target in azimuth direction, and we correct the cross-track baseline of the channel 2 echo signal according to the actual arrangement of the two receiving telescopes [17].

By means of phase compensation, we make the channel 2 echo signal equivalent to the echo signal received by the telescope located along the track. The formula of cross-track phase compensation is

$$\varphi_p(t_m) = -\frac{4\pi}{\lambda} [r_1(t_m + \Delta t_m) - r_2(t_m) - (R_1 - R_2)], \quad (2)$$

$$\Delta t_m = -\frac{B_Y}{V_t}, \quad (3)$$

where  $B_Y$  is the length of equivalent along-track baseline,  $V_t$  is the along-track velocity of the target,  $t_m$  is slow time,  $r_1$  and  $r_2$

present the distances between the moving target and two receiving telescopes, and  $R_1$  and  $R_2$  present the distance between center of the scene and two receiving telescopes.

### B. Motion Phase Error Compensation

Because the laser echo signal is easily affected by motion, the long-time echo signal with rough Doppler frequency compensation is divided into multiple sub-apertures, and the motion phase error and further Doppler frequency of each sub-aperture are compensated, respectively, which can effectively reduce the influence of large motion bandwidth on imaging.

Motion phase error compensation is referred to as motion compensation for short in this paper. The coarse compensation and along-track interferometry [9–12] were adopted to remove the influence of motion phase error on echo signals. The instantaneous Doppler frequency caused by motion can be estimated through the time-frequency analysis of echo signals, and the coarse compensation of the motion phase error can be realized. During along-track interferometry, the radial velocity of the target is estimated through dual-channel echo signals obtained along the track, the instantaneous Doppler frequency is calculated, and the precise compensation of the motion phase error is realized. The formulas of along-track interferometry are as follows:

$$V_r = -\frac{\lambda V_t \Delta \varphi}{2\pi B_Y}, \quad (4)$$

$$\Delta f_d = -\frac{2\Delta V_r}{\lambda}, \quad (5)$$

where  $V_r$  is radial velocity of the target,  $\Delta \varphi$  is the interferometric phase of dual-channel echo signals, which are aligned in slow time direction, and  $\Delta V_r$  and  $\Delta f_d$  are instantaneous radial velocity variation and instantaneous Doppler frequency variation caused by motion.

### C. Sub-Aperture Imaging and Geometric Correction

After dividing sub-apertures of echo signals, the RD algorithm is applied, and the imaging results of multiple sub-apertures are stitched. Considering short sub-apertures, range cell migration correction can be ignored in the process of imaging. Geometric correction of the stitched image is realized by Stolt transformation. In order to improve the imaging effect, range-direction super-resolution and multi-look processing in azimuth direction can be added in the imaging process.

## 4. SIMULATION AND EXPERIMENTAL DATA PROCESSING

### A. Parameters of Simulation and Experiment

Experimental photos and experimental scene models are shown in Figs. 8 and 9. We choose a car at the size of 4.6 m × 1.7 m × 1.5 m as the cooperative target, which is pasted with multiple 4.5 cm × 2 cm high-reflectivity paper. The cooperative target moves along the negative direction of the Y axis and passes through the pitching beam expanded laser spot.



**Fig. 8.** Photos of the cooperative target and the laser spot. (a) Photo of the cooperative target. (b) Photo of the laser spot taken by the infrared camera.

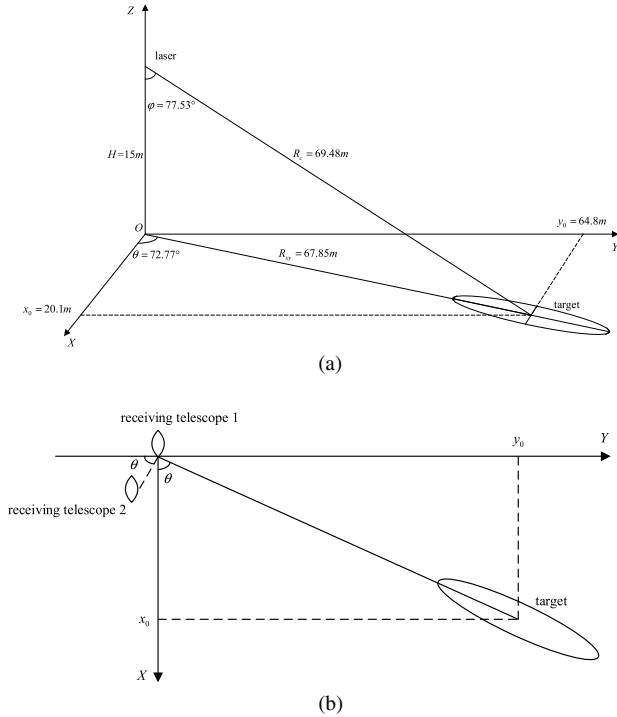


**Fig. 9.** Experimental scene and distribution of receiving telescopes.

After beam expansion in pitching direction, the laser beam width in pitching direction and azimuth direction is 34.9 mrad and 1.5 mrad, respectively. Because the laser beam irradiates the cooperative target at a large squint angle, the projected azimuth beam coverage is 0.3 m.

When the main component of the moving phase error is sinusoidal, its instantaneous Doppler frequency change formula [9] is

$$\varphi(t_m) = -\frac{4\pi}{\lambda} \Delta R(t_m) = -\frac{4\pi}{\lambda} A \sin(2\pi f_m t_m + \varphi_m), \quad (6)$$

$$\Delta f_d(t_m) = \frac{1}{2\pi} \frac{d\varphi(t_m)}{dt_m} = -\frac{4\pi}{\lambda} f_m A \cos(2\pi f_m t_m + \varphi_m), \quad (7)$$

where  $\lambda$  is wavelength of the laser,  $\Delta R(t_m)$  is radial distance variation of the target caused by motion, and  $A$ ,  $f_m$ , and  $\varphi_m$  are amplitude, frequency, and initial phase of sinusoidal radial distance variation, respectively. Combined with the transmitting reference signal, the range-direction pulse compression

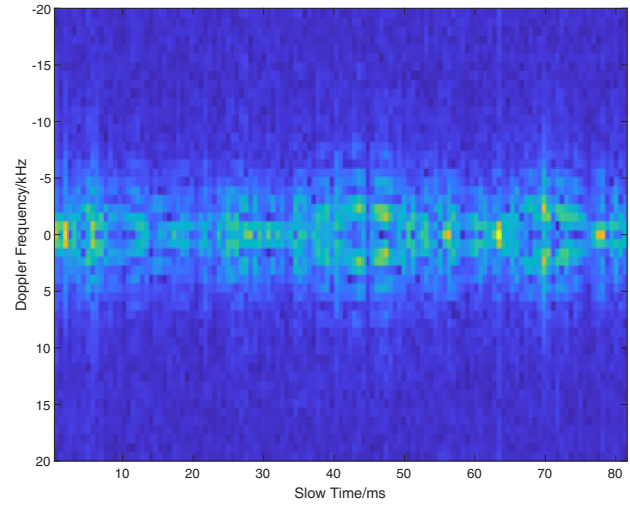


**Fig. 10.** Time-frequency analysis result of the static vehicle echo signal after range-direction pulse compression.

result of static target echo signal can be obtained, and its time-frequency analysis result is shown in Fig. 10. According to the time-frequency analysis, the Doppler frequency range of motion coverage is 6 kHz, the motion frequency is 37 Hz, and the motion amplitude is 20  $\mu\text{m}$ .

## B. Simulation and Analysis

The imaging simulation of the laser echo signal is based on the spatial imaging in the case of large squint angle as shown in Section 3, and experimental parameters of the laser echo signal are shown in Table 1.

Because of the laser's characteristics of high frequency and short wavelength, the laser echo signal is easily affected by motion phase error. The sinusoidal radial distance error of the target is introduced to simulate the influence of motion phase error on laser echo signals.

As shown in Fig. 11, the locations of point targets in the simulation scene are set according to the actual distribution of high-reflectivity paper on the cooperative target. The coverage ranges of point targets in X, Y, and Z directions are 1.7 m, 1.6 m,

**Table 1.** Simulation Parameters of Laser Echo Signal Imaging

Parameter	Value
Laser length	1.55 $\mu\text{m}$
Along-track equivalent baseline length	8.15 mm
Squint angle	72.77°
Distance	69.48 m
Azimuth beam width	1.5 mrad
Projected azimuth spot size	0.3 m
Radial velocity of target	4.95 m/s
Doppler frequency	6.39 MHz
Transverse velocity of target	5.3 m/s
Synthetic aperture time	0.057 s
Pulse repetition rate	100 kHz
Fast time sampling rate	4 GHz
Motion frequency	37 Hz
Motion amplitude	20 $\mu\text{m}$

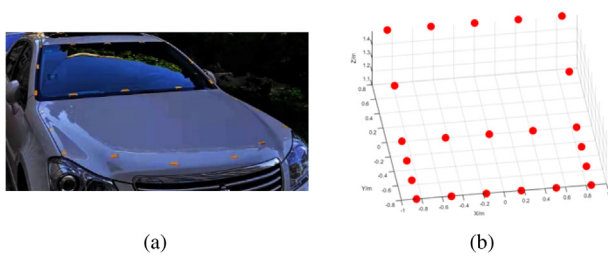


**Fig. 11.** Distribution of point targets in the experiment and simulation. (a) Photo of high-reflectivity paper distribution on the cooperative target. (b) Distribution of point targets in simulation.

and 0.4 m, respectively. The spacing between adjacent point targets in X direction is 0.34 m and 0.425 m, the spacing between adjacent point targets in Y direction is 0.4 m and 0.27 m, and the coordinates of target points in Z direction are 1.1 m, 1.3 m, and 1.5 m.

The range-direction pulse compression results of echo signals with noise, motion phase error estimation of 1 sub-aperture, imaging result, and interferometric phase and coherence coefficient of the imaging results of dual-channel signals without/with motion compensation are shown in Fig. 12. According to Figs. 12(e)–12(h), which are the interferometric phase and coherence coefficient of the imaging results without range-direction super-resolution and azimuth-direction multi-look processing, the stability of the interference phase and the improvement of the coherence coefficient after motion compensation indicate that the coarse compensation and track-path interferometry can effectively compensate the motion phase error.

Solid boxes in Fig. 12(i) mark the corresponding positions of point targets in the imagine results of the experimental data shown in Fig. 13, and the dotted box mark the corresponding location of Fig. 12(j). According to the simulation parameters in Table 1, the synthetic aperture time is 0.057 s, and the azimuth bandwidth of the echo signal is 3.66 kHz, so the ideal Y-direction (azimuth-direction) resolution of the imaging result is 1.45 mm. After range-direction super-resolution and azimuth-range multi-look processing, the resolutions of the imaging result in X direction and Y direction are 1.06 cm and 2.66 cm.

**C. Experimental Data Processing**

In the experiment, the cooperative target passes through the laser spot in Y direction at a transverse velocity of 5.3 m/s, and the slow time chirp-rate of the echo signal is 64.175 kHz/s. When the sub-aperture time is set to 81.92 ms, the ideal Y-direction (azimuth direction) resolution of the imaging result is 2 mm.

The range-direction pulse compression results, time-frequency analysis and motion phase error estimation of the sub-aperture of the actual dual-channel echo signals and the interferometric phase and coherence coefficient of imaging results without/with motion compensation are shown in Fig. 13. According to Figs. 13(a)–13(d), it is obvious that duration of the echo signal is 1.2 s and the motion bandwidth reaches about 30 kHz. For the convenience of display, Fig. 13(c) is

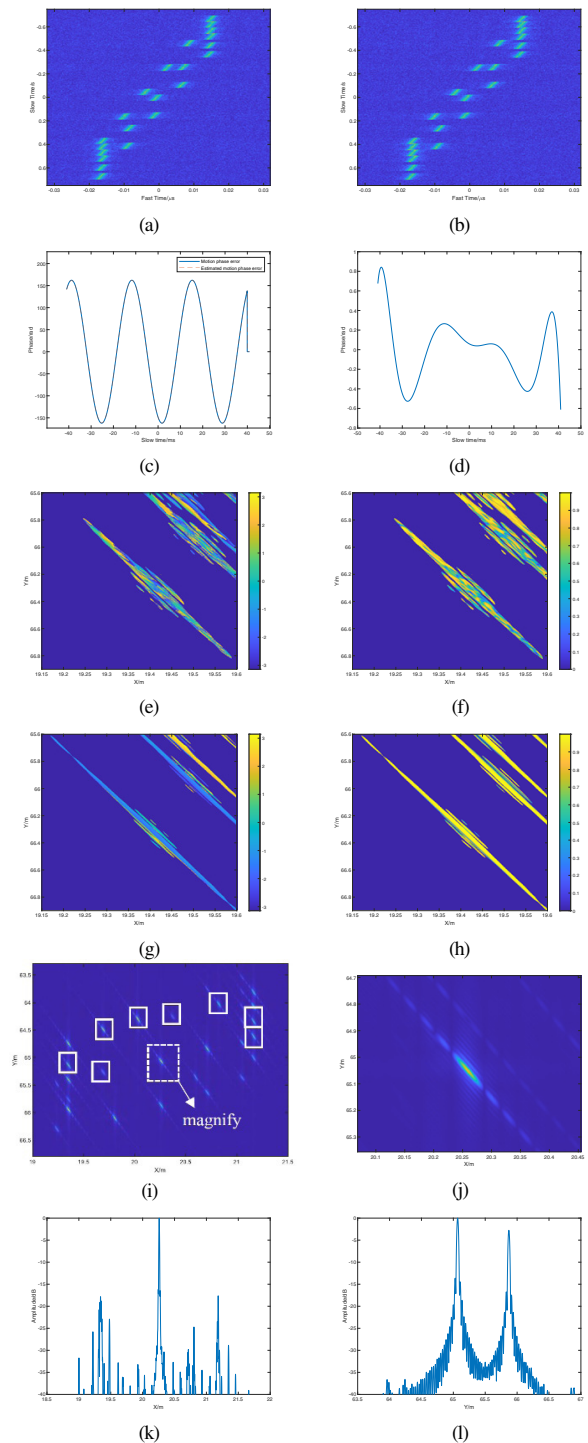


**Fig. 12.** Simulation results of laser echo signal imaging. (a) Range-direction pulse compression result of channel 1 echo signal. (b) Range-direction pulse compression result of channel 2 echo signal. (c) Motion phase error estimation of the sub-aperture. (d) Error of the sub-aperture motion phase error estimation. (e) Interferometric phase of partial imaging results without motion compensation. (f) Correlation coefficient of partial imaging results without motion compensation. (g) Interferometric phase of partial imaging results with motion compensation. (h) Correlation coefficient of partial imaging results with motion compensation. (i) Imaging result. (j) Magnified partial imaging result. (k) Section of the imaging result in X direction. (l) Section of the imaging result in Y direction.

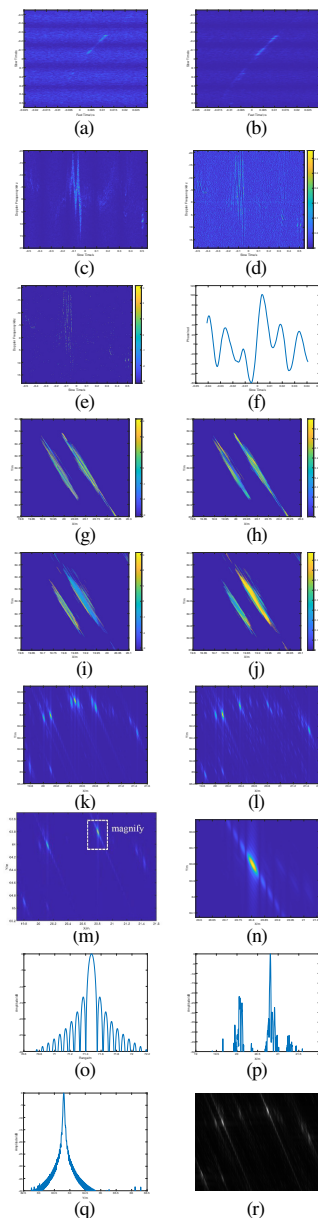


**Fig. 13.** Experimental data processing results. (a) Range-direction pulse compression result of channel 1 echo signal. (b) Range-direction pulse compression result of channel 2 echo signal. (c) Coherent superposition of multiple range gate time-frequency analysis of the channel 2 echo signal. (d) Coherence coefficient of time-frequency analysis of dual-channel echo signals. (e) Interferometric phase of time-frequency analysis of dual-channel echo signals. (f) Error of the sub-aperture motion phase error estimation. (g) Interferometric phase of partial imaging results without motion compensation. (h) Correlation coefficient of partial imaging results without motion compensation. (i) Interferometric phase of partial imaging results with motion compensation. (j) Correlation coefficient of partial imaging results with motion compensation. (k) Imaging result of channel 2 echo signal without motion compensation. (l) Imaging result of channel 1 echo signal with motion compensation. (m) Imaging result of channel 2 echo signal with motion compensation. (n) Magnified partial imaging result of channel 2 echo signal. (o) Section of the imaging result of channel 2 echo signal in range direction. (p) Section of the imaging result of channel 2 echo signal in X direction. (q) Section of the imaging result of channel 2 echo signal in Y direction. (r) Processed incoherent superposition of dual-channel imaging results.

the time-frequency analysis of coherent superposed channel 2 echo signal of multiple range gates with range cell migration correction. It can be seen that there exists complex motion phase error in the echo signal, and the coarse compensation of motion phase error can be realized by estimating Doppler frequency curve through time-frequency analysis. Figures 13(d) and 13(e) indicate that the motion phase errors in dual-channel echo signals have a good coherence, and it is reasonable to estimate the motion phase error through along-track interferometry.

Comparing the interferometric phase and coherence coefficient of dual-channel imaging results without/with motion compensation when range-direction super-resolution and azimuth direction multi-look processing are not applied, the stable interferometric phase and large coherence coefficient of the imaging results with motion compensation indicate that the motion compensation method based on the coarse compensation and along-track interferometry can effectively solve the high resolution imaging problem of ISAL with motion errors.

After range-direction super-resolution, geometric correction, and azimuth direction multi-look processing, the coverage ranges of point targets in X direction and Y direction are 1.6 m and 1.8 m, respectively. The resolutions of imaging results in range direction, X direction, and Y direction are 6.77 cm, 1.22 cm, and 3.74 cm, respectively. The processed incoherent superposition of the dual-channel imaging results is shown in Fig. 13(r), and it indicates that there exist eight point targets in the imaging results of the experimental data. Considering factors such as experimental error, the distribution error of the point targets in simulation, and the different reflection directions of high-reflectivity paper due to the uneven cooperative target and the space-variant problem, the distribution of point targets in imaging results of the experimental data is basically consistent with the distribution of partial point targets in simulation shown in Fig. 12(i), which are marked by solid boxes.

## 5. CONCLUSION

The dual-channel ISAL imaging experimental system based on wide-pulse BPSK signals and the spatial imaging of laser echo signals of the moving target with small computation and large squint angles are introduced in this paper. The effectiveness of the imaging method is verified through the simulation and experimental data processing. Based on the low side-lobe characteristic of BPSK signals and the range-direction pulse compression with the transmitting reference signal, the main-sidelobe ratio of the echo signals of the static target and the moving target can reach 25 dB and 15 dB, respectively. Combining pulse compression of BPSK signals and range-direction super-resolution, the range-direction resolution of experimental data imaging results can reach the order of 6 cm, illustrating the application value of the BPSK signal in SAL/ISAL imaging.

The motion phase error compensation is realized with the coarse compensation and along-track interferometry combined in this paper. The time-frequency analysis of dual-channel echo signals and their interferometry indicate the rationality of this method. The comparison of the interferometric phase

and coherence coefficient of dual-channel imaging results with-out/with motion compensation prove the effectiveness of this method.

Because of the high far-field sidelobe of the BPSK signal, the imaging quality is influenced to some extent in the condition of wide-pulse signals. In further research, sidelobe suppression methods can be introduced to improve the imaging quality.

**Funding.** Key Deployment Projects of Chinese Academy of Sciences (E03701010F).

**Disclosures.** The authors declare no conflicts of interest.

**Data availability.** Data underlying the results presented in this paper are not publicly available at this time but may be obtained from the authors upon reasonable request.

## REFERENCES

1. S. Crouch and Z. Barber, "Laboratory demonstrations of interferometric and spotlight synthetic aperture radar techniques," *Opt. Express* **20**, 24237–24246 (2012).
2. Z. Zhao, J. Huang, S. Wu, K. Wang, T. Bai, Z. Dai, X. Kong, and J. Wu, "Experimental demonstration of tri-aperture differential synthetic aperture radar," *Opt. Commun.* **389**, 181–188 (2017).
3. J. Buck, B. Krause, A. Malm, and C. Ryan, "Synthetic aperture imaging at optical wavelengths," in *Conference on Lasers and Electro-Optics and Conference on Quantum electronics and Laser Science Conference* (IEEE, 2009).
4. B. Krause, J. Buck, C. Ryan, D. Hwang, P. Kondratko, A. Malm, A. Gleason, and S. Ashby, "Synthetic aperture radar flight demonstration," in *Conference on Lasers and Electro-Optics (CLEO): Laser Science to Photonic Applications* (2011), pp. 1–2.
5. X. Xu, S. Gao, and Z. Zhang, "Inverse synthetic aperture radar demonstration and outdoor experiments," in *China International SAR Symposium (CISS)* (2018).
6. J. Du, D. Li, and M. Ma, "Performance analysis and image processing of phase-modulated signal on airborne synthetic aperture radar," *J. Radars* **3**, 111–118 (2014).
7. Z. Zhao, Y. Su, J. Wu, H. Duan, S. Wu, and W. Huang, "Synthetic aperture radar imaging via synthetic frequency-stepped linearly-chirping signal," *High Power Laser Part. Beams* **27**, 21–26 (2015).
8. F. Li, H. Zhang, J. Wu, G. Hong, W. Xu, and Z. Shu, "Mechanism and experiment of code intensity-modulation on synthetic aperture radar," *Infrared Laser Eng.* **44**, 2575–2582 (2015).
9. M. Ma, D. Li, and J. Du, "Imaging of airborne synthetic aperture radar under platform vibration condition," *J. Radars* **3**, 591–602 (2014).
10. H. Xuan and D. Li, "Vibration phases estimation based on multi-channel interferometry for ISAL," *Appl. Opt.* **57**, 6481–6490 (2018).
11. D. Li, K. Zhou, A. Cui, M. Qiao, S. Wu, Y. Wang, Y. Yao, J. Wu, and J. Gao, "Multi-channel inverse synthetic aperture radar imaging detection technology and experimental research," *Laser Optoelectron. Prog.* **58**, 1811017 (2021).
12. X. Hu, D. Li, and J. Du, "Image processing for GEO object with 3D rotation based on ground-based InISAL with orthogonal baselines," *Appl. Opt.* **58**, 3974–3985 (2019).
13. Y. Lu and G. Zhou, "A low sidelobe m-sequence code set for pulse compression radar," *J. Tsinghua Univ.* **1988**, 23–30 (1988).
14. G. Sun, G. Liu, and H. Gu, "Signal analysis and processing for random binary phase coded pulse radar," *J. Syst. Eng. Electron.* **15**, 520–524 (2004).
15. Y. Hu, Y. Zhen, X. Geng, and Y. Deng, "Doppler compensation for phase-coded signals," *J. Electron. Inf. Technol.* **31**, 2596–2599 (2009).
16. A. Korshunov, L. Fridman, and E. Sinitin, "Analysis of influence of Doppler frequency shift on effectiveness of phase-shift keyed signal compression," in *36th International Conference on Telecommunications and Signal Processing (TSP)* (IEEE, 2013).
17. J. Du, D. Li, M. Ma, X. Hu, and M. Qiao, "Vibration estimation and imaging of airborne synthetic aperture radar based on interferometry processing," *Chin. J. Lasers* **43**, 253–264 (2016).